PRAMANA — journal of physics

Vol. 85, No. 2
August 2015
pp. 227–238

# A new prompt heavy-ion-induced fission mode

W UDO SCHRÖDER
Departments of Chemistry and Physics, University of Rochester, Rochester, NY 14627, USA
E-mail: schroeder@chem.rochester.edu

**DOI:** 10.1007/s12043-015-1031-7; ***e*Publication:** 19 July 2015

**Abstract.** Fission instabilities induced by mechanical and thermal stresses on intermediate nuclear systems in heavy-ion reactions are poorly understood but should reveal independent evidence for the nuclear equation of state (EoS), notably the tensile strength of finite nuclei. Experimental evidence is presented in support of a new mode of prompt fission of the composite nucleus formed in central $^{78}$Kr+$^{40}$Ca collisions at only a few MeV per nucleon above the interaction barrier. The new process recalls the 'L-window for fusion' phenomenon, which was predicted by the early reaction theory and reappears in modern DFT model calculations.

**Keywords.** Heavy ions; fusion–fission; L-window.

**PACS Nos 25.70.Pq; 25.70.Mn**

## 1. Introduction

Over the past three quarters of a century following the discovery [1–3] of nuclear fission, this process has been studied intensely for a range of medium-weight to heavy nuclei, mostly at low excitation energies and spins [4–7]. Major research goals have been to explore the stability of nuclear droplets [8,9] and to map adiabatic pathways of fission in a multidimensional space of macroscopic shapes [3,10–14], significantly influenced by mean-field symmetries [4,15–17].

In spite of impressive theoretical progress, it has so far proven very difficult to explain, within a comprehensive theoretical framework, the evolution of fission or fission-like modes observed [18–24] since many years for nuclear systems produced with significant transfers of excitation energy, linear and angular momenta, or for nuclei far away from the valley of stability [25]. Well-documented examples of such processes are the emission of (one or several) nuclear clusters ('intermediate-mass fragments') in fission and heavy-ion reactions, known [26] to be energetically possible long before they were observed. Later statistical models of the so-called multifragmentation (see e.g. [27–29]) asserted a nuclear 'liquid–gas phase transition,' rather than a fission-like process.

But these models relied on highly disputable, ad-hoc assumptions regarding spatial confinement of nuclear systems, methods which are still sometimes used in theoretical studies (e.g., [30]) of fission barriers at finite nuclear temperatures.

Another type of essentially binary nuclear disintegration of projectile-like fragment (PLF), target-like fragment (TLF) or intermediate dinuclear system (DNS) in heavy-ion reactions is apparently dominated by dynamics, rather than statistics of compound nuclear decay. Some reported examples are the snapping of the matter bridge ('neck') between nascent reaction fragments [31,32], a process akin to ternary fission [4,33] and the binary splitting of one or both of the main fragments following a dissipative reaction, occurring still within the range of substantial Coulomb and nuclear interactions [18,19,34–36].

While the field of nuclear fission research still has a range of questions to investigate, it is already possible to use fission phenomenology and quantitative systematics as diagnostic tools for investigating nuclear fusion and dissipation processes, as well as to probe the nuclear mean-field 'equation of state' (EoS), specifically the nuclear tensile strength and its transformation with isospin, excitation energy and spin. Section 2 is meant to provide motivation for the study of EoS-related physics that can be explored in heavy-ion-induced fission or fission-like processes. Section 3 reports the experimental observations of an apparently new dynamic (shock-induced) fission process that does not proceed through a compound nucleus (CN) stage. Section 4 offers a summary and outlook.

## 2. Motivation: Heavy-ion-induced fission and the EoS

Interest in heavy-ion reactions, specifically fusion–fission, at bombarding energies safely above the interaction barrier derives from their potential to map the (meta-) stability domain of finite nuclei in terms of $A/Z$ ratio, excitation energy and angular momentum. Fusion–fission reactions above the barrier provide experimental constraints to the nuclear mean field, the EoS, which can be realized in macroscopic interaction potentials or, microscopically, in terms of density ($\rho$), spin ($\sigma$) and isospin ($\delta$) dependent energy functional $\epsilon(\rho, \sigma, \delta)$. The EoS can be tested differently in both the entrance (fusion) and the exit (fission) channels. The exit channel system may experience effective fields resulting from single-particle and/or collective excitation modes depending on the internal damping of initial disturbances of the matter distribution. Therefore, such models that treat entrance and exit channels on the same footing and are able to follow the system trajectory are desirable, in particular when it does not proceed through a CN state, where most information on nuclear dynamics would be lost.

In simple approximation, the multidimensional entrance-channel mean field for two interacting nuclei ($Z_1$, $A_1$) and ($Z_2$, $A_2$) is modelled in terms of an effective potential energy $V(r, \ell)$ depending on the nuclear centre separation distance $\mathbf{r}$, relative angular momentum $\ell$ and reduced mass $\mu$. It is given by a sum of Coulomb, nuclear and centrifugal potentials, e.g.,

$$V(r, \ell) = \frac{e^2 Z_1 Z_2}{r} + V_{\mathrm{N}}(r) + \frac{\hbar^2 \ell(\ell+1)}{2\mu r^2}. \tag{1}$$

As an example, the effective potential for $^{16}$O+$^{208}$Pb is plotted in figure 1 vs. $\mathbf{r}$ and for various partial waves with angular momentum $\ell$. Here, the nuclear potential $V_{\mathrm{N}}$ is taken

as the proximity potential [37,38], which is based on the finite-range Seyler–Blanchard energy density. Schematic trajectories in figure 1 are drawn to illustrate dynamic inhibition of fusion in the $^{16}$O+$^{208}$Pb entrance channel effected by compressional 'bounce-off' (trajectory 1), by deflection of the system trajectory away from the CN fusion path (trajectory 3) by driving forces favouring mass or shape asymmetry [39] or by strong dissipation. Only one of those pictured (trajectory 2) is trapped inside a potential 'pocket,' leading to at least temporary capture and, with a probability of $P_{\mathrm{CN}}$, to an equilibrated CN behind the unconditional saddle in the actually multidimensional potential energy surface (e.g., [9]).

For mass-asymmetric systems and bombarding energies above a barrier in $V(r,\ \ell)$ well-defined, e.g., in terms of the proximity interaction model and prevailing strong one-body frictional forces [38,40], it is expected that fusion occurs (figure 1, trajectory 2) for partial waves from $\ell = 0$ up to a critical value $\ell = \ell_f$. This implies an approximately triangular cross-section distribution $\mathrm{d}\sigma_f/\mathrm{d}\ell \propto \ell \cdot T_\ell(E) \cdot P_{\mathrm{CN}}(\ell, E)$, with entrance-channel transmission coefficient $T_\ell(E) \sim \Theta(\ell_{\mathrm{g}} - \ell)$ admitting all partial waves up to the grazing angular momentum $\ell_{\mathrm{g}}$. The function $P_{\mathrm{CN}}(\ell, E)$ defines the fusion range as a 'window' $[0, \ell_f]$. It represents the probability for relaxation [39] of the dinuclear entrance-channel configuration into an equilibrated CN. This leads to a CN fusion cross-section of

$$\sigma_f(E) = \frac{\pi\hbar^2}{2\mu E}\left\{\sum_{\ell=0}^{\infty}(2\ell+1)\cdot T_\ell(E)\cdot P_{\mathrm{CN}}(\ell, E)\right\}. \tag{2}$$

The upper $\ell$ wave domain with a probability $\bar{P}_{\mathrm{CN}}(\ell, E) = 1 - P_{\mathrm{CN}}(\ell, E)$ corresponds to dissipative and quasifission reactions. The excited CNs produced at the lower range

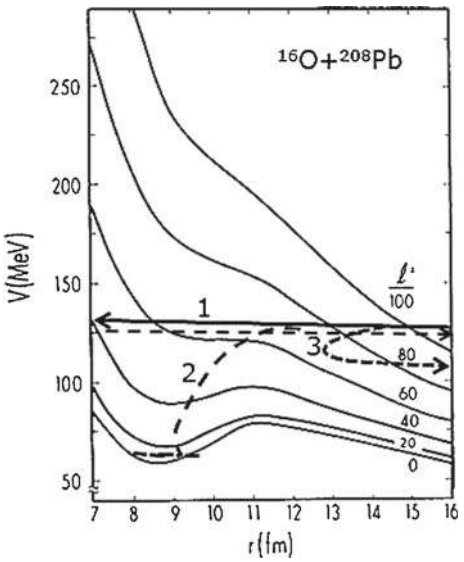


**Figure 1.** Radial dependence of effective $^{16}$O+$^{208}$Pb interaction potential for different partial waves with angular momentum $\ell$. Trajectory labels indicate elastic bounce-off (1), capture (2) and a dissipative reaction process (3).

within the fusion window [0, $\ell_{\rm ER}$] subsequently decay statistically, via the emission of light particles into evaporation residues (ER); for the higher $\ell$ waves fission occurs. The competition between these two decay processes is thought to be governed by the angular momentum stability criteria of the rotating liquid-drop model (RLDM) [8].

In contrast to expectations of $P_{\rm CN} \approx 1$ for a band of low $\ell$ waves, $0 \leq \ell \leq \ell_f$, at energies above the barrier, TDHF model calculations of the 1970s and 1980s [41–43] predicted the so-called 'L-window for fusion' for certain light systems and energies of a few MeV per nucleon. An example is given in figure 2, where the CN fusion range is shown hatched in the $E_{\rm c.m.}$–$\ell$ plane [42]. While the upper $\ell$-wave boundary is immediately plausible, the one forbidden for the more central collisions is less obvious. Apparently, insufficient nuclear stopping power in head-on collisions allows the projectile and the target nuclei to pass through one another, emerging back-to-back at a 180° c.m. angle relatively unscathed.

As the experimental search for such an L-window has remained unsuccessful (e.g., [40,43]), the realism of the early TDHF calculations appeared challenged with respect to computational technique, accuracy and completeness. It is therefore significant and interesting that modern self-consistent time-dependent density functional (TDDF) calculations [44,45] using density functional theory [46] predict a similar transparency effect in central fusion-type heavy-ion collisions. In figure 3, results of such calculations with Skyrme-type (SLy5) functionals are illustrated, showing three snapshots of the density contours of the projectile- and target-like fragments in a central ($\ell = 0$) $^{78}$Kr + $^{40}$Ca collision at $E/A = 11$ MeV, along with the fragment velocity directions. This is the actual system for which experimental results are discussed in §3.

The above TDDF calculations predict a prompt asymmetric fission mode to be established at times of the order of a few 100 fm/c after touching in the entrance channel. The corresponding period of this dynamic fission mode, and the associated energy scale of 3–5 MeV, are characteristics of single-particle motion but quite uncharacteristic of regular CN fission, which should be a slow collective process. The few calculations that have been performed to-date with the TDDF model suggest [44] the existence of an energy threshold for transparency, as well as sensitivity to the assumed EoS and to the entrance channel configuration of the possibly deformed projectile and the target nuclei.

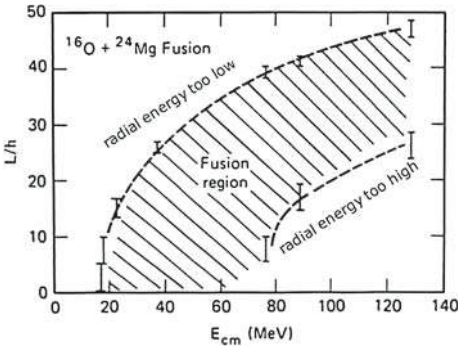


**Figure 2.** Theoretical (TDHF) prediction for the energy-L region in which complete fusion should occur (hatched) for the $^{16}$O+$^{24}$Mg reaction (figure taken from [42]).

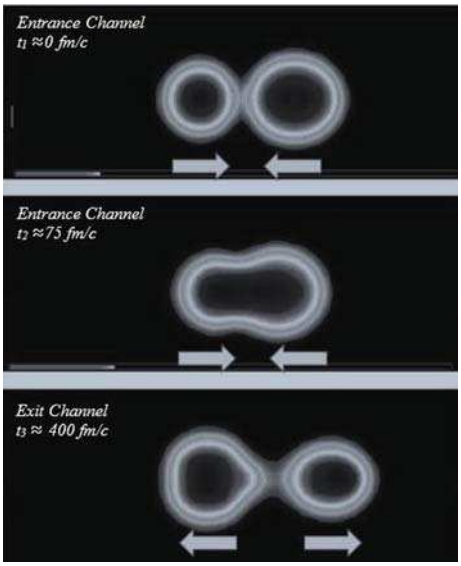


**Figure 3.** Density contours of projectile- and target-like fragments in central $^{78}$Kr+$^{40}$Ca collisions at $E/A = 11$ MeV predicted by TDDF calculations [44]. Figure shows the snapshots for the indicated reaction times $t_1$–$t_3$.

In this context, related theoretical efforts should be identified, which consider particular mechanisms for fusion inhibition at low energies and/or for heavy systems in terms of a deflection away from the fusion path by mass-asymmetric driving forces [39,47,48] or by diabatic repulsion [47–49]. Presumably, there are experimental observables such as fragment angular distributions and correlations that would allow one to distinguish experimentally between the various mechanisms.

While there are quite a few microscopic studies of the dependence of dynamic fission modes on mass-to-charge ratio (isospin), excitation and entrance-channel angular momentum, qualitative to semiquantitative expectations can be formulated based on the underlying nuclear EoS. A highly simplified EoS, based on Skyrme-type energy functionals, is illustrated in figure 4 for various neutron ($\rho_n$) to proton ($\rho_p$) density excesses $I$. It has the form

$$\epsilon(\rho, I) = \epsilon_0(\rho) + C_I I^2; \quad I = \frac{\rho_n - \rho_p}{\rho} \tag{3}$$

with $C_I$ a parameter related to the symmetry energy and

$$\epsilon_0(\rho) = \langle E/A \rangle \approx \underbrace{\langle E_{kin}/A \rangle}_{(3/5)\epsilon_f} \left(\frac{\rho}{\rho_0}\right)^{2/3} + a\left(\frac{\rho}{\rho_0}\right) + b\left(\frac{\rho}{\rho_0}\right)^{5/3}. \tag{4}$$

Here, $\rho_0$ is the saturation nuclear matter density, and the quantities $a$ and $b$ are constants. The associated nuclear tensile strength is defined as the minimum of the (negative) internal pressure $P = \rho^2(\partial\epsilon/\partial\rho) \leq 0$. It has been estimated [50] as $P_{int}^{min} \approx -0.7$ MeV/fm$^3$ for symmetric matter ($N = Z$). Asymmetric matter, featuring an excess of like nucleons, $|I| > 0$, is less stable than the symmetric matter as illustrated

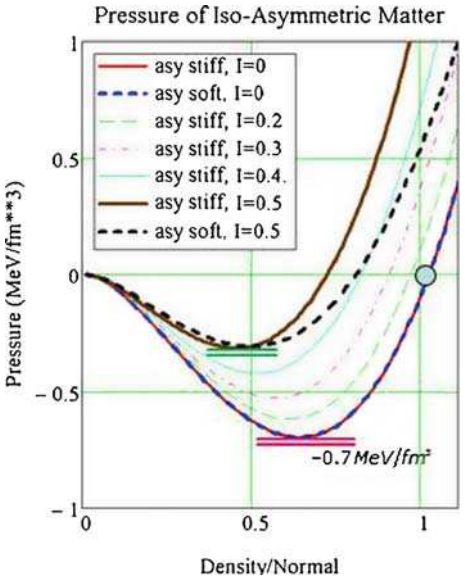


**Figure 4.** Thermal pressure $P$ vs. matter density $\rho/\rho_0$, for different overall neutron excesses $\langle I\rangle = (N-Z)/A$, based on a Skyrme-type nuclear EoS. The tensile strength is indicated by horizontal bars for different values of $\langle I\rangle$.

in figure 4 for a range of large neutron excesses. Similarly, thermal excitation reduces the tensile strength, thus providing less nuclear cohesion.

Once the tensile strength is exceeded, e.g., by an internal pressure surge or by an external load on the nuclear surface, nuclear matter promptly loses cohesion and disintegrates. The former dynamic fission-like event could be induced by compression/rarefaction waves following collisional impact shock, as suggested by the TDDF calculations [44] discussed earlier. The latter event could arise from the opposing interaction and inertial forces. For cold, symmetric nuclear matter, such a dynamic fission-like splitting can be initiated in heavy-ion reactions already at low relative energies, (1–2) MeV above the barrier [50]. It would certainly be very interesting to find out experimentally, what the parameters are that describe the influence of the EoS on dynamical fission and its damping at substantial excitations.

A host of experimental studies of low-energy fission [4–7] have demonstrated the predictive power of the RLDM [8], for the onset of nuclear shape instability with increasing angular momentum $J$, and of Bohr's compound nucleus model for the competition between fission and particle decay modes. However, as soon as the excitation energy $E^*/A$ exceeds a few MeV per nucleon, these models appear to break down, and new fission-like instabilities appear. There is mounting evidence that new modes, like multiple cluster emission, are associated with the dynamics and thermodynamics of nuclear expansion.

In a series of studies on excited nuclei in vacuum, treated [51,52] in the appropriate open microcanonical statistical ensemble, it was noticed that, because of its high local level density, the nuclear surface plays an important role in this thermal expansion. The fact that an excited dinuclear 'daughter' system has much more surface and associated

surface entropy than an excited 'parent' mononucleus of the same $A$, $Z$ and total energy, is the cause for a very fast, 'prompt' split of the parent nucleus. The physical reasons for such behaviour are understood from the fundamental proposition of the microcanonical statistical approach: given a total excitation energy, $E^*_{\rm tot}$, the nucleus expands to assume a new equilibrium density profile $\rho_{\rm eq}$, cooling down in the process and ending at maximum entropy $S$,

$$\left(\frac{\partial S}{\partial \rho}\right)_{E^*_{\rm tot}} = 0 \rightarrow \left\{ \begin{array}{c} \rho_{\rm eq} \\ T \end{array} \left( \begin{array}{c} \text{microcanonical} \\ \text{model} \end{array} \right) . \right. \tag{5}$$

Here, the microcanonical temperature $T$ is defined via the density of states. Entropy $S$ and thermal part, $\mathrm{E}^*_{\rm th}$, of the nuclear excitation energy are approximately related by

$$S = 2\sqrt{aE^*_{\rm th}} \quad \text{with} \quad E^*_{\rm th} = E^*_{\rm tot} - E^*_{\rm conf}, \tag{6}$$

where $a$ represents the nuclear level density parameter ('little $a$'), which has a volume and an important surface contribution [53]. The entropy, defined in eq. (6), depends directly on the configurational portion of the excitation energy part, $E^*_{\rm conf}$, containing all energy differences relative to the ground state, such as due to expanded volume, shape differences and finite angular momentum $J \neq 0$. Obviously, the nuclear EoS enters the calculation of $E^*_{\rm conf}$ in a significant fashion, because dilution of the matter density away from saturation consumes excitation energy.

The main effect of the expansion degree of freedom on nuclear fissility for excitations of more than a few MeV per nucleon stems from the softening of the nuclear surface region and the disappearance of the surface tension, which is quite dramatic [52] above $E^*/A \geq 4.5$ MeV. This effect implies a reduction of the critical angular momentum where, according to the RLDM [8], nuclear droplet shapes become unstable, and binary fission disappears altogether already at moderately high excitations. Better understanding of the fission process at high excitations requires the development of a RLDM for hot nuclei and specific experimental tests.

## 3. Experiments

Fission processes induced in the inverse-kinematic $^{78,86}$Kr + $^{40,48}$Ca reactions at $E_{\rm lab}/A = 10$ MeV/A have been studied by the University of Rochester group [54] in conjunction with the ISODEC Collaboration. The objective in the inverse-kinematics reaction $^{78}$Kr + $^{40}$Ca at $E_{\rm lab}/A = 10$ MeV/A was to search at forward angles for dynamical fission-like or splitting events observed in other reactions [34,35,55]. For orientation, the RLDM predicts loss of stability for the medium-weight composite system ($A_{\rm tot} = 118$, $Z_{\rm tot} = 56$) against distortions from spherical shape for angular momenta above $J \approx 60$ ($\hbar$).

In the experiments, pulsed Kr beams produced by the LNS Catania K800 cyclotron were used to bombard the self-supporting calcium targets of appropriate thicknesses (1 mg/cm$^2$). Charged products were detected with the 1192 Si–CsI(Tl) telescopes of the CHIMERA $4\pi$ multidetector array [56]. The data acquisition system provided $\Delta E/E$ energy, time-of-flight ($\delta t \sim 1$ ns) and pulse shape information, the latter only for a subset of Si detectors.

Figure 5 displays an experimental correlation between the atomic numbers of two detected fragments ($Z_i > 3$) on a log scale. Narrow distributions trailing from $Z_i \approx 36$ and 16, clearly visible in the diagram, are attributed to projectile-like and target-like fragments, respectively, from the dissipative Kr+Ca collisions. Of interest to the following are the events in the cross-section ridge at $Z_1 + Z_2 \approx 48 \pm 2$, adding up to 85% of the total charge of the system ($Z_{\rm tot} = 56$). However, the sum charge is shared between the two correlated fragments in terms of a very broad distribution peaking at symmetric splits. The corresponding mass correlations are also obtained for the same events, with $A_1 + A_2 \approx 106 \pm 16$. Similar to the appearance of $Z_{\rm tot}$ distribution in figure 5, the distribution of the sum of the masses of correlated fragments is also much narrower than the distribution in mass splits.

The evidence discussed earlier strongly suggests a fusion–fission process as the origin of the correlated fragments. This conclusion is strongly supported by all the remaining fusion–fission type observables. For example, the measured c.m. folding-angle distribution of velocity vectors indicates collinear, back-to-back emission of the fragments. The individual fragment velocity vectors $\vec{v}_1^L$, $\vec{v}_2^L$ and the corresponding momenta are used to determine the corresponding velocity components, parallel and perpendicular to the beam, in the rest frame of the emitter, the fissioning source. The resulting invariant velocity plot is given in figure 6 for symmetric fragments with fission-like relative velocities. The origin of this plot is taken as the velocity $\vec{v}_{\rm cms}$ of the c.m. system in the laboratory.

From the fact that this experimental velocity plot is centred at the origin, one concludes that the correlated fragments originate indeed from the composite nucleus, which is at rest in the overall c.m. system and contains the entire system mass and the entire linear momentum. A slight deformation of the velocity distribution is observed in beam direction whereas the spectrum of transversal relative velocities is isotropic.

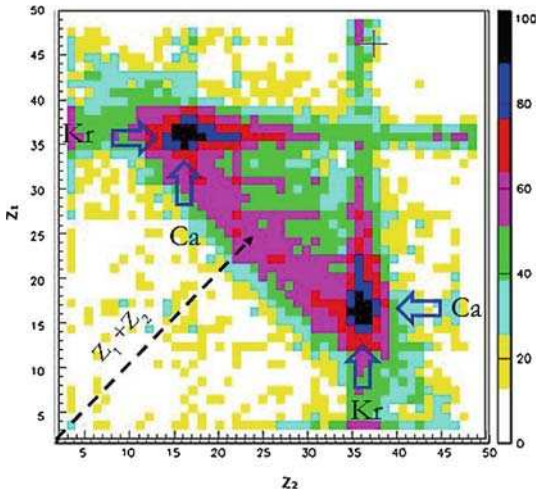


**Figure 5.** Typical charge correlations $Z_1$ vs. $Z_2$ measured at $\theta = 5°$ for the $^{78}$Kr+$^{40}$Ca reaction at 10 A MeV. Plotted is the log of $\mathrm{d}^2\sigma/\mathrm{d}Z_1Z_2$ in arbitrary units. Arrows and labels identify the domains of projectile- and target-like nuclei.

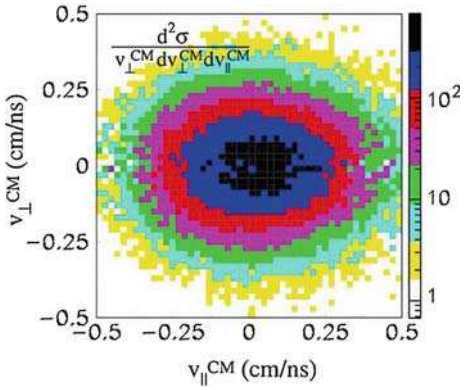


**Figure 6.** Correlated fragment velocities parallel and perpendicular to the beam, in the rest frame of the emitter. Fragment with relative velocities in the gate defined in figure 7 are included. The velocity of the c.m. system in the laboratory has been subtracted.

The spectrum of relative fragment velocities $v_{\rm rel} = \left|\vec{v}_1^L - \vec{v}_2^L\right|$ is shown in figure 7. It is obviously bimodal, showing one distinct peak centred at $v_{\rm rel} = 4.5$ cm/ns which is attributed to the dissipative reaction component. Of particular interest in the present context is the second component peaking at the much lower velocity of $v_{\rm rel} = 2.4$ cm/ns, slightly larger than what is characteristic of equilibrium fission. The vertical bars in figure 7 indicate the velocity range accepted in the definition of fission-like events included in the velocity plot of figure 6. There is, obviously, a small contamination of this velocity domain by the tail of a component due to dissipative collisions. Therefore, for all intents and purposes, the correlated fragments described previously come from a fusion–fission-like process. Its somewhat unusual properties include the shape of the fragment angular distributions, which is strongly anisotropic, except for mass-symmetric events, not symmetric at 90°.

The experimental fission angular distribution of the heavy fragment, $d\sigma/d\Theta_{\rm HFr}$, is plotted in figure 8. Different symbols represent the indicated different ranges in fission fragment mass asymmetry defined as $\eta_A = (A_1 - A_2)/(A_1 + A_2)$. For symmetric events,

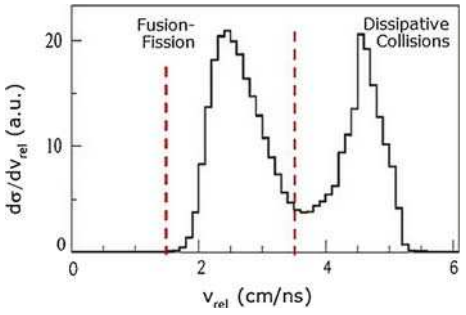


**Figure 7.** Distribution of relative velocities of correlated events in the $^{78}$Kr+$^{40}$Ca reaction at $E/A = 10$ MeV. A collinearity condition of $-1.0 < \cos(\alpha) < -0.7$ (see figure 6) was imposed on the fragments.

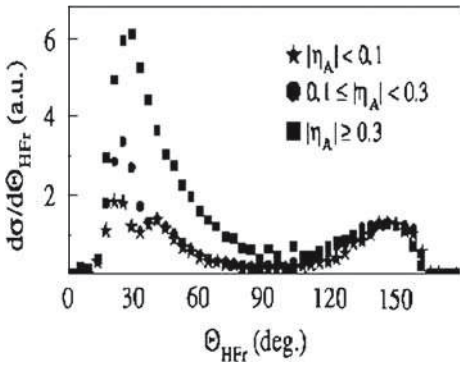


**Figure 8.** Angular distributions of the larger (of the two) fragments in the centre-of-mass system for three bins in mass asymmetry $\eta_A$, normalized to yields at backward angles.

$|\eta_A| < 0.1$, the distribution is seen to be symmetric at about $\Theta_{\rm HFr} = 90°$, as expected. But it is not isotropic and has maxima both at forward and backward angles. This behaviour indicates a rather strong alignment of the fission axis in the beam direction and demonstrates the dominantly dynamic character of the process. A weak contribution from the regular CN fission to the ensemble of considered events is not excluded; its contribution can be estimated from the cross-section around 90°. For asymmetric fission events, the heavier of the fragments is emitted forward preferentially in the c.m. system. This is a very unusual observation.

Fragments are emitted in the process with significant excitation, as can be detected by their sequential evaporation of particles. In the experiment, sequential emission of $\alpha$-particles from the excited fission fragments was identified by the characteristic Galilei-invariant $\alpha$-particle velocity distributions plotted with respect to the corresponding fragment emission direction. The scatter plot velocity distribution shown in figure 9

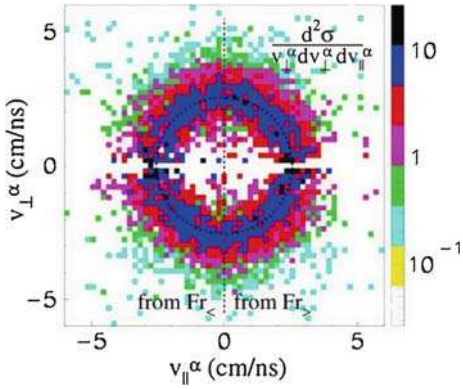


**Figure 9.** Galilei-invariant velocity distribution of $\alpha$-particles emitted from correlated mass-symmetric fission fragments. The parallel and perpendicular components are defined relative to the fragment velocity vectors.

is a composite of events in which $\alpha$-particles from the forward going fragment populate the half plane $v_{\parallel}^{\alpha} > 0$, and those from the backward going fragment are plotted in the region $v_{\parallel}^{\alpha} < 0$. The resulting good matching of the two semicircular velocity patterns demonstrates the correctness of the identification of the emitters, as well as the quality of experimental calibrations.

As is already evident from the approximately constant invariant $\alpha$-particle cross-section in figure 9, the spin angular momentum of the emitting fragments is negligibly small, which identifies the central collisions, i.e., $\ell \approx 0$. This conclusion was shown to apply consistently to events emitted in good alignment of their fission axis with the beam direction, regardless of mass asymmetry. In contrast, fission fragments emitted in lateral directions are associated with anisotropic $\alpha$-particle angular distributions, indicating significant intrinsic spin values $J$, as expected for equilibrium statistical fission.

## 4. Conclusions

There is evidence for a dynamical fission-like process in which the composite system formed in central collisions with total mass, charge and linear momentum bypasses the compound nuclear equilibrium, at least partially, undergoes an essentially binary split into a broad mass and charge distribution. Strong memory of the beam direction is retained in a strongly aligned scission axis, with heavier fragments in asymmetric splits are preferentially emitted in the direction of flight of the projectile. The process is reminiscent of events predicted in microscopic theoretical calculations. The inability of the system to completely stop the relative motion appears to set limits on the tensile strength of the underlying nuclear equation of state.

## Acknowledgements

The author acknowledges the work by his colleagues, J Tõke, H Singh, M J Quinlan, E Henry and S Nyibule, as well as the contribution by members of the ISODEC Collaboration. He thanks V E Oberacker and A S Umar for providing results of their TDDF calculations prior to publication. The work was supported by US DOE Grant No. DE-FG02-88ER4014.

## References

[1] O Hahn and F Strassmann, *Naturwiss.* **27**, 11 (1939)
[2] L Meitner and O R Frisch, *Nature* **143**, 239 (1939)
[3] N Bohr and J A Wheeler, *Phys. Rev.* **56**, 426 (1939)
[4] R Vandenbosch and J R Huizenga, *Nuclear fission* (Academic Press, New York and London, 1973)
[5] C Wagemans, *The nuclear fission process* (CRC Press, Boca Raton, 1991)
[6] M Dasgupta *et al*, *Annu. Rev. Nucl. Part. Sci.* **48**, 401 (1998) and references therein
[7] B B Back *et al*, *Rev. Mod. Phys.* **86**, 317 (2014) and references therein
[8] S Cohen, F Plasil and W J Swiatecki, *Ann. Phys. (NY)* **82**, 557 (1974)
[9] P Møller *et al*, *Phys. Rev. C* **79**, 064304 (2009) and references therein
[10] A Bohr, *Mat.-Fys. Medd. Dan. Vid. Selsk* **26**, 14 (1952)

[11] W D Myers and W J Swiatecki, *Nucl. Phys.* **81**, 1 (1966)
[12] S Cohen and W J Swiatecki. *Ann. Phys. (NY)* **19**, 67 (1962); *ibid*. **22**, 406 (1963)
[13] P Møller and J Nix, *Nucl. Phys. A* **229**, 269 (1974)
[14] W D Myers, *Droplet model of atomic nuclei* (Plenum Press, New York, 1977)
[15] S G Nilsson, *Kgl. Dan. Vid. Selsk., Mat.-Fys. Medd.* **29**, (No. 16) (1955)
[16] V M Strutinsky, *Nucl. Phys. A* **95**, 420 (1967); *ibid*. *A* **122**, 1 (1968)
[17] M Brack *et al*, *Rev. Mod. Phys.* **44**, 320 (1972)
[18] P Glaessel *et al*, *Phys. Rev. Lett.* **48**, 1089 (1982)
[19] D v Harrach *et al*, *Phys. Rev. Lett.* **48**, 1093 (1982)
[20] W U Schröder and J R Huizenga, *Treatise in heavy-ion physics* edited by D A Bromley (Plenum Press, New York, 1984) Vol. 2, p. 113
[21] J Tõke *et al*, *Nucl. Phys. A* **440**, 327 (1985)
[22] L G Moretto and G J Wozniak, *Prog. Part. Nucl. Phys.* **21**, 401 (1988)
[23] D J Hinde *et al*, *J. Phys.: Conf. Ser.* **420**, 012115 (2013)
[24] W Gawlikowicz *et al*, *Phys. Rev. C* **81**, 014604 (2010)
[25] S Hofmann and G Münzenberg, *Rev. Mod. Phys.* **72**, 733 (2000)
[26] W J Swiatecki, *Proc. Sec. Int. Conf. Peaceful Uses Atom. En.* (Geneva, 1958) Vol. 15, p. 248
[27] D H E Gross, *Rep. Prog. Phys.* **53**, 605 (1990)
[28] D H E Gross, *Eur. Phys. J. A* **30**, 293 (2006)
[29] J P Bondorf *et al*, *Phys. Rep.* **133**, 133 (1995)
[30] J C Pei *et al*, *Phys. Rev. Lett.* **102**, 192501 (2009)
[31] U Brosa *et al*, *J. Phys. G* **10**, 933 (1984); *Nucl. Phys. A* **502**, 423c (1989)
[32] M Colonna *et al*, *Nucl. Phys. A* **642**, 449 (1998)
[33] I Halpern, *Annu. Rev. Nucl. Sci.* **21**, 245 (1971)
[34] S Hudan *et al*, *Phys. Rev. C* **70**, 031601 (2004); *ibid*. *C* **71**, 054604 (2005)
[35] H Singh *et al*, *Proc. IWMF11, EPJ Web of Conf.* **31**, 14 (2012)
[36] J Wilzcynski *et al*, *Phys. Rev. C* **81**, 024605 (2010)
[37] J Blocki, J Randrup, W J Swiatecki and C F Tsang, *Ann. Phys. (NY)* **105**, 427 (1977)
[38] J Randrup, *Nucl. Instrum. Methods* **146**, 213 (1977)
[39] W J Swiatecki, K Siwek-Wilczynska and J Wilczynski, *Phys. Rev. C* **71**, 014602 (2005)
[40] J R Birkelund *et al*, *Phys. Rep.* **56**, 107 (1979)
[41] S E Koonin, K T R Davies *et al*, *Phys. Rev. C* **15**, 1359 (1977)
[42] J Krieger *et al*, *Phys. Rev. C* **24**, 928 (1981)
[43] U Mosel, *Treatise in heavy-ion science* edited by D A Bromley (Plenum Press, New York and London, 1984) Vol. 2, p. 1
[44] V E Oberacker and A S Umar, Private communication (2014)
[45] A S Umar *et al*, *J. Phys. G: Nucl. Part. Phys.* **37**, 064037 (2010)
[46] A D Becke, *J. Chem. Phys.* **98**, 5648 (1993); *ibid*. **140**, 18A301 (2014) and references therein
[47] A Diaz-Torres, *Nucl. Phys. A* **652**, 61 (1999)
[48] A Diaz-Torres, *Phys. Rev. C* **74**, 064601 (2006)
[49] W Nörenberg, *Nucl. Phys. A* **409**, 191 (1983)
[50] G F Bertsch and D Mundinger, *Phys. Rev. C* **17**, 1646 (1978)
[51] J Tõke and W U Schröder, http://arXiv:nucl-th/9810063, *Rev. Lett.* **82**, 5008 (1999)
[52] J Tõke and W U Schröder, *Phys. Lett. B* **734**, 364 (2014) and references to earlier work
[53] J Tõke and W J Swiatecki, *Nucl. Phys. A* **372**, 141 (1981)
[54] E Henry *et al*, *INFN-Lab. Naz. Sud Activity Report* **723**, 19 (2013)
[55] M J Quinlan, Ph.D. Thesis (Univ. Rochester, 2012), http://gradworks.umi.com/34/78/3478351.html
[56] A Pagano *et al*, *Nucl. Phys. A* **734**, 504 (2004)